PHYSICAL REVIEW E **91**, 022718 (2015)

Statistics of a neuron model driven by asymmetric colored noise

Finn Müller-Hansen,[1,2,*] Felix Droste,[1,3] and Benjamin Lindner[1,3]

[1]*Bernstein Center for Computational Neuroscience, Haus 2, Philippstraße 13, 10115 Berlin, Germany*

[2]*Department of Physics, Freie Universität Berlin, Arnimallee 14, 14195 Berlin, Germany*

[3]*Department of Physics, Humboldt Universität zu Berlin, Newtonstraße 15, 12489 Berlin, Germany*

(Received 25 September 2014; published 27 February 2015)

Irregular firing of neurons can be modeled as a stochastic process. Here we study the perfect integrate-and-fire neuron driven by dichotomous noise, a Markovian process that jumps between two states (i.e., possesses a non-Gaussian statistics) and exhibits nonvanishing temporal correlations (i.e., represents a colored noise). Specifically, we consider asymmetric dichotomous noise with two different transition rates. Using a first-passage-time formulation, we derive exact expressions for the probability density and the serial correlation coefficient of the interspike interval (time interval between two subsequent neural action potentials) and the power spectrum of the spike train. Furthermore, we extend the model by including additional Gaussian white noise, and we give approximations for the interspike interval (ISI) statistics in this case. Numerical simulations are used to validate the exact analytical results for pure dichotomous noise, and to test the approximations of the ISI statistics when Gaussian white noise is included. The results may help to understand how correlations and asymmetry of noise and signals in nerve cells shape neuronal firing statistics.

DOI: 10.1103/PhysRevE.91.022718 PACS number(s): 87.18.Tt, 87.19.lc, 05.40.−a

I. INTRODUCTION

Excitable systems driven by noise play an important role in various fields, such as laser physics, biophysics, physical chemistry, and neuroscience [1]. In essence, an excitable system remains silent after a weak stimulus but responds to a sufficiently strong perturbation by a stereotypical pulse (spike). A main objective of theory is to develop methods to calculate the statistics of these spikes for various cases of stochastic forcing.

In particular, stochasticity in excitable neural systems has attracted a lot of attention because it may play a functionally important role in the processing of information [1–4]. On the level of single neurons, fluctuations stem from intrinsic noise in the processing of action potentials, such as synaptic unreliability [5] and ion channel noise [6]. On the network level, cortical neurons receive input from several thousands of other neurons, which can be mimicked by an effective random input [7,8].

Most studies of stochastic neuron models have focused on uncorrelated Gaussian input (for a review, see [9,10]). Different types of neuron models driven or perturbed by Gaussian noise with short or vanishing correlation time have been thoroughly studied, and statistical properties have been derived analytically [1,11,12]. However, neuronal input is in general neither temporally uncorrelated (it is a *colored* and not a *white* noise) nor does it possess Gaussian statistics. Pronounced input correlations in time arise because of temporally correlated input stimuli, presynaptic refractoriness or bursting, network up-down states, or short-term synaptic plasticity. Correlated and non-Gaussian random inputs are usually more difficult to treat analytically. Most studies on correlated noise have focused on low-pass-filtered Gaussian inputs [11–17] (for an exception with band-pass-filtered Gaussian noise, see [18]). Analytical studies on temporally uncorrelated non-Gaussian stimuli in the form of white shot noise can be found in Refs. [7,19–21].

To our knowledge, Markovian dichotomous noise is one of the rare analytically accessible cases of a temporally correlated non-Gaussian neural input [16,22,23]. Such noise (also known as the telegraph process) jumps between two discrete states with constant rates and has been used in physics for a long time to study the effect of noise correlations on nonlinear dynamical systems [24–29]. It can also be used to test the influence of an asymmetry of the input noise on the statistics of the driven system.

The aim of this paper is to better understand the effect of non-Gaussian correlated noise on neuronal firing. We use the perfect integrate-and-fire (PIF) neuron model driven by dichotomous noise to investigate the influence of correlations and asymmetry in the input on the statistics of the output spike train. The PIF model adequately describes the statistics of some neurons in the tonically firing regime [18,30,31]. Due to its simple dynamics, the PIF model allows us to derive closed expressions for its statistical properties, a feature that integrate-and-fire models do not have in general.

In the neurobiological context, dichotomous noise is particularly suitable to mimic up-down state input. Up-down states are activity patterns of neural populations that are found in the cortices of many mammalian species [32–34]. They are characterized by alternating periods of neural spiking (up state) and virtually no firing (down state). Of course, a pure two-valued input is a gross oversimplification of any neural input. Hence, we also take weak uncorrelated fluctuations around the two states into account.

The output spike train of a neuron can be described by various statistics. In this paper, we focus on three measures: (i) The probability distribution of the interspike interval (ISI), (ii) the correlation coefficient among ISIs, and (iii) the power spectrum of the spike train.

In Ref. [16], the probability density and correlation coefficient of the ISI was derived analytically for a PIF neuron driven by a symmetric dichotomous noise (equal transition

*f.mueller-hansen@posteo.de

rates). Here, we extend this analytical framework in two ways: First, we consider asymmetric dichotomous noise that can have two different transition rates. On average, it thus stays longer in one preferred state than in the other one. This generalization is of special interest because neural input such as that resulting from network up-down states is in general not symmetric. Second, we examine the effect of a mixture of dichotomous and Gaussian noise on the ISI statistics. The use of additional Gaussian white noise is motivated by the presence of intrinsic noise and by deviations of real input from an ideal two-state process.

This paper is organized as follows: In the second section, we introduce the PIF neuron model and the statistical measures. In the following sections, we discuss the ISI distribution, the ISI correlations, and the power spectrum. Each of these sections starts with an analytic derivation of the respective measure for the case of driving with pure dichotomous noise. Subsequently, we discuss the results and illustrate characteristic features. For the ISI density and ISI correlations, we also introduce approximations for additional white noise. All of our analytical results are compared with stochastic simulations. We conclude with a brief discussion of our results.

II. NEURON MODEL AND STATISTICAL MEASURES

This paper considers the perfect integrate-and-fire neuron. It belongs to the model class of integrate-and-fire neurons, which describe a neuron only by its membrane voltage v. Instead of an active spike generation mechanism, the model has a spike-and-reset rule. Accordingly, the model registers a spike whenever the membrane potential reaches a threshold voltage v_T. Then, the voltage is reset to the reset potential v_R. A first-order differential equation describes the dynamics of the membrane voltage. This equation becomes a stochastic differential equation if a noise process drives the neuron model.

To simplify notation, we set the membrane time constant $\tau_m = 1$. The time is therefore measured in units of τ_m. A combination of a constant input current μ, a dichotomous noise process $\eta(t)$, and white noise with intensity D drive the PIF model. For this setup, the stochastic differential equation describing the voltage dynamics reads

$$\dot{v}(t) = \mu + \eta(t) + \sqrt{2D}\xi(t), \tag{1}$$

where $\xi(t)$ is Gaussian white noise with autocorrelation $\langle \xi(t)\xi(t')\rangle = \delta(t-t')$. To keep the equations simple, we set the reset potential to zero. Because the right-hand side of Eq. (1) is independent of v, we can shift v such that $v_R = 0$ without reformulating the problem. The threshold voltage too could be rescaled such that $v_T = 1$. For the generality of our final formulas, we keep the parameter v_T in the following calculations.

The dichotomous noise process $\eta(t)$ is characterized by two discrete states. Without loss of generality, we consider in this paper a process that jumps between the values $+\sigma$ and $-\sigma$; two arbitrary values σ_+ and σ_- can always be shifted by a constant c such that $\sigma_\pm = c \pm \sigma$, and c can be lumped into μ. In the following, we limit the analysis to the case in which $\mu > \sigma > 0$, and thus

$$\mu \pm \sigma > 0. \tag{2}$$

This implies that the voltage can cross the threshold in both states of the dichotomous noise. The case in which the voltage can pass the threshold only in the $+\sigma$ state is tractable [23] but less interesting because serial correlations vanish (see below).

The dichotomous process jumps between the states with two different transition probabilities (rates). The transition rates are labeled λ_+ for jumps from the plus to the minus state and λ_- vice versa. If $\lambda_+ \neq \lambda_-$, the mean residence times $\tau_\pm = 1/\lambda_\pm$, i.e., the mean time between a jump into a state and the following jump out of it, differ. This results in an asymmetry between the two states. Therefore, this process is called asymmetric dichotomous noise. If the two rates are equal, the mean residence times are the same and we call the process symmetric dichotomous noise.

To quantify the asymmetry between the rates, we introduce the parameter u that can take values between -1 and 1 and is defined as

$$u = \frac{\lambda_- - \lambda_+}{\lambda_- + \lambda_+}. \tag{3}$$

This parameter helps to shorten notation and thus appears in the following calculations. By setting $u = 0$, we can recover the special case of symmetric dichotomous noise.

The asymmetry u is closely related to the mean and the variance of the asymmetric dichotomous process:

$$\langle \eta \rangle = u\sigma, \quad \langle \Delta\eta^2 \rangle = \sigma^2(1-u^2). \tag{4}$$

Furthermore, the skewness of the dichotomous noise γ_{DN} is given by

$$\gamma_{\mathrm{DN}} = \frac{-2u}{\sqrt{1-u^2}}. \tag{5}$$

The stationary dichotomous process is characterized by an exponentially decaying autocorrelation function [24]

$$C(\tau) = \langle \eta(t)\eta(t+\tau)\rangle - \langle \eta(t)\rangle^2 = \sigma^2(1-u^2)e^{-|\tau|/\tau_c}. \tag{6}$$

However, the higher-order correlation functions of dichotomous noise differ from those of exponentially correlated Gaussian noise, i.e., the Ornstein-Uhlenbeck process. The correlation time τ_c appearing in Eq. (6) is proportional to the inverse of the mean transition rate λ,

$$\tau_c = \frac{1}{2\lambda} \quad \text{with} \quad \lambda = \frac{1}{2}(\lambda_+ + \lambda_-), \tag{7}$$

and, together with the variance, determines the intensity of the dichotomous noise defined as $D_{\mathrm{DN}} = \tau_c \langle \Delta\eta^2 \rangle$.

Figure 1 shows a realization of dichotomous noise and the corresponding voltage trajectories of the PIF model with and without white noise. In the absence of white noise [Fig. 1(b)], the voltage has only two different slopes corresponding to the two noise states. Figure 1(c) shows the effect of additional Gaussian white noise on the voltage for the same realization of dichotomous noise. Figure 2 illustrates different asymmetries of the dichotomous noise and their effect on the voltage and the spiking.

The statistics of the point process generated by the model can be characterized in different ways. Neuroscientists often

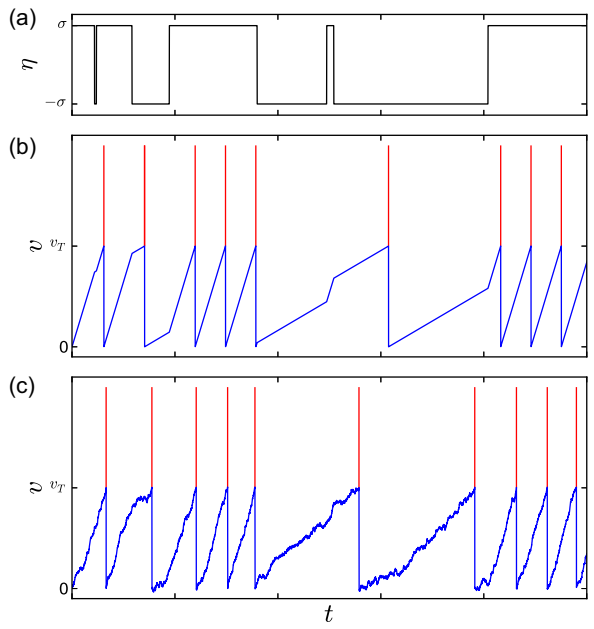

FIG. 1. (Color online) Illustration of the voltage dynamics of the PIF model. (a) Realization of dichotomous noise. (b) Simulation of the voltage driven by this realization. (c) As (b) but with additional weak Gaussian white noise ($D = 0.01$). The spikes (horizontal lines exceeding v_T, red) were added for a better illustration of spike times. Parameters: $\sigma = 0.7, \lambda = \mu = v_T = 1, u = -0.5$.

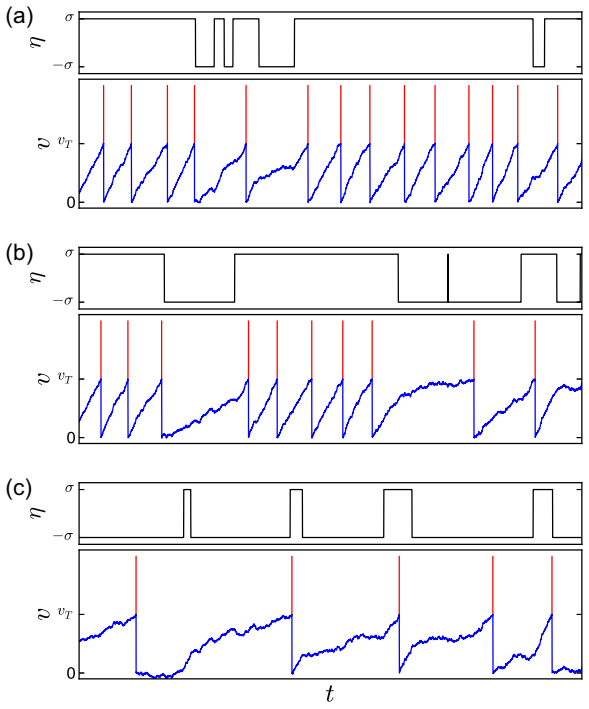

FIG. 2. (Color online) Different asymmetries of the dichotomous noise process. (a) Positive asymmetry $u = 0.6$. (b) Symmetric dichotomous noise $u = 0$. (c) Negative asymmetry $u = -0.6$. Remaining parameters as in Fig. 1(c).

consider the statistics of the interspike intervals (ISIs) $I_j = t_j - t_{j-1}$, in which t_j is the time instant of the jth spike. More generally, we may also consider sums of n subsequent ISIs or nth-order intervals [7], defined as $T_n^j = \sum_{k=0}^{n-1} I_{j+k}$. In the next sections, we derive analytical expressions for the probability distribution of the nth-order interval and its moments. By setting $n = 1$, we obtain the distribution and moments for the ISI.

Another statistic of interest is the correlation among ISIs that can be quantified by the serial correlation coefficient

$$\rho_k = \frac{\langle I_{j+k} I_j \rangle - \langle I_{j+k} \rangle \langle I_j \rangle}{\langle I_j^2 \rangle - \langle I_j \rangle^2}, \tag{8}$$

which measures correlations between two intervals with lag k, i.e., that are $(k-1)$ ISIs apart. The serial correlation coefficient (SCC) is normalized to values between -1 and 1. A positive SCC indicates that on average long ISIs follow long ones and/or short ISIs short ones. A negative SCC points at a statistic where short ISIs succeed long ones and/or vice versa.

Instead of interval statistics, we may also consider the statistics of the spike train, $x(t) = \sum_i \delta(t - t_i)$, in particular its power spectrum, which describes the frequency distribution of the variance,

$$S(\omega) = \lim_{T \to \infty} \frac{\langle \tilde{x}(\omega) \tilde{x}^*(\omega) \rangle}{T}. \tag{9}$$

Here $\tilde{x}(\omega) = \int_0^T dt\, x(t) e^{i\omega t}$ is the Fourier transform of the spike train, and the angular brackets indicate an ensemble average over all noise processes involved.

In the following, we provide detailed derivations of analytical expressions for the nth-order interval distribution, the ISI correlations, and the power spectrum.

III. PROBABILITY DENSITY OF THE NTH-ORDER INTERVAL

For the simple PIF model, the determination of the nth-order interval distribution constitutes a first-passage-time (FPT) problem for the voltage variable. Put differently, this distribution equals the probability density of the time needed to reach the threshold for the first time after starting at the reset value. The nth-order interval density can be calculated because the dynamics of the PIF model [Eq. (1)] is independent of the membrane voltage v itself. Therefore, the time the voltage needs to go n times from the reset $v_R = 0$ to the threshold $v = v_T$ with the reset mechanism in place is equivalent to the time it takes to go one time from the reset to the threshold $v = n v_T$ [16]. This property allows us to compute the nth-order interval distribution by solving the first-passage-time problem with the threshold $n v_T$. We start with the problem in the absence of white noise ($D = 0$), for which we denote the probability density of the nth-order interval by $J_{\mathrm{D},n}(T_n)$ (D in the index stands for the dichotomous noise). At the end of the section, we will also present an approximation of the density $J_{\mathrm{D+W},n}(T_n)$ in the presence of both dichotomous and Gaussian white noise.

By $P_\pm(v,t)$ we denote the probability density to find the system at time t in the plus or minus state around the voltage v. Then, Eq. (1) without white noise (i.e., $D = 0$) has the

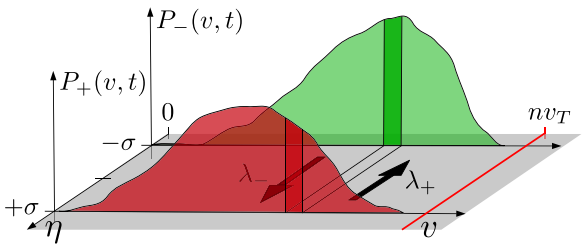

FIG. 3. (Color online) Illustration of the first-passage-time problem in state space at one point in time. The probability distributions P_- and P_+ evolve in time according to Eqs. (10) and (11). Apart from drifting in the v direction, probability can also flow from P_+ to P_- and vice versa. The first-passage-time distribution corresponds to the probability current at the threshold nv_T.

following associated master equations [35]:

$$\partial_t P_+ = \lambda_- P_- - \lambda_+ P_+ - (\mu+\sigma)\partial_v P_+, \tag{10}$$

$$\partial_t P_- = \lambda_+ P_+ - \lambda_- P_- - (\mu-\sigma)\partial_v P_-. \tag{11}$$

The resulting time evolution of the probability densities P_+ and P_- is illustrated in Fig. 3. The first-passage-time problem from $v=0$ to $v=nv_T$ is associated with the solution of the above master equation in the presence of an absorbing boundary at $v=nv_T$. More specifically, given the correct initial conditions, the nth-order interval distribution $J_{\mathrm{D},n}(T_n)$ is equivalent to the probability current in the v direction,

$$J(v,t) = (\mu+\sigma)P_+(v,t) + (\mu-\sigma)P_-(v,t), \tag{12}$$

taken at the absorbing threshold $v=nv_T$,

$$J_{\mathrm{D},n}(T_n) = J(nv_T, T_n). \tag{13}$$

The initial conditions for this problem have to fulfill two characteristics: (i) At $t=0$, all trajectories start at the reset voltage $v_R=0$. (ii) For a stationary spike train, the probability for the initial value of the noise has to be self-consistent, i.e., the initial distribution of noise states at the reset has to be equal to the distribution of the noise at the threshold (noise upon firing), $p_F(\eta)$.

The stationary probability $p_{\mathrm{DN},\pm}$ to find the dichotomous noise in either the plus or the minus state is

$$p_{\mathrm{DN},\pm} = \tfrac{1}{2}(1\pm u). \tag{14}$$

The probability to cross the threshold is higher when the dichotomous noise is in the plus state because in this state the voltage moves faster toward the threshold. Thus, the probability density of the noise upon firing is proportional to the velocity of the voltage in the respective noise state. We obtain after normalization

$$p_F(\pm\sigma) = \frac{\mu\pm\sigma}{\mu+u\sigma}\, p_{\mathrm{DN},\pm}. \tag{15}$$

In line with the assumption Eq. (2), trajectories always move in the positive v direction. Hence, the voltage cannot cross the threshold multiple times, and the evolution of the probability density in the presence of an absorbing boundary is the same as that in the absence of such a boundary. Put differently, we may use the freely evolving solution of the equation.

Equations (10) and (11) can be reduced to a second-order equation,

$$\left[\partial_t^2 + 2\lambda\partial_t + 2\mu\partial_v\partial_t + 2\lambda(\mu+u\sigma)\partial_v + (\mu^2-\sigma^2)\partial_v^2\right]P_\pm = 0, \tag{16}$$

where we have used for notational ease the mean transition rate λ and the asymmetry parameter u of the dichotomous noise [cf. Eq. (4)]. To find a solution of Eq. (16), we first transform the equation via the Galilean transformation $v\to v-\mu t$ to a frame of reference where $\mu=0$. Second, as was done previously in Ref. [36], we remove the asymmetry by applying a Lorentz transformation known from special relativity:

$$v' = \gamma(v-u\sigma t), \quad t' = \gamma\left(t-\frac{uv}{\sigma}\right), \tag{17}$$

$$\lambda' = \frac{\lambda}{\gamma}, \quad \gamma = \frac{1}{\sqrt{1-u^2}} = \frac{\lambda}{\sqrt{\lambda_+\lambda_-}}. \tag{18}$$

Ultimately, we arrive at the second-order differential equation known as the telegrapher's equation,

$$\left(\partial_{t'}^2 + 2\lambda'\partial_{t'} - \sigma^2\partial_{v'}^2\right)P_\pm = 0. \tag{19}$$

The general solution of this equation for arbitrary initial conditions can be found in [37, p. 868]. For our purpose, we need the conditional probability densities $P_{\eta_0,\eta}(v,t|0,0)$ denoting the probability to find a trajectory at time t around v and in the noise state $\eta=\pm\sigma$ provided it was at time zero at $v=0$ and the dichotomous noise was in state η_0. To this end, we have to transform the solution of Eq. (19) back to the original variables t and v. The normalized probability densities read

$$P_{\pm\sigma,\pm\sigma}(v,t|0,0) = e^{-\lambda\left(t-\frac{uv}{\sigma}\right)}\left[\delta(v\mp\sigma t) + \frac{\lambda\Theta}{2\gamma\sigma\alpha(v,t)}(\sigma t\pm v)I_1\left(\frac{\lambda\alpha(v,t)}{\gamma\sigma}\right)\right], \tag{20}$$

$$P_{\pm\sigma,\mp\sigma}(v,t|0,0) = e^{-\lambda\left(t-\frac{uv}{\sigma}\right)}\frac{\lambda\Theta}{2\sigma}(1\mp u)I_0\left(\frac{\lambda\alpha(v,t)}{\gamma\sigma}\right), \tag{21}$$

where $\alpha(v,t)=\sqrt{\sigma^2t^2-v^2}$ and $\Theta=\theta(\sigma t-|v|)$ with the Heaviside step function $\theta(x)$. $\delta(x)$ is the Dirac delta function and $I_b(x)$ denotes the modified Bessel function of the first kind and order b.

Applying the Galilean back transformation simply replaces v by $v-\mu t$ in these expressions. The initial states are distributed according to the noise upon firing, so that

$$P_\pm(v,t) = \sum_{\eta_0} p_F(\eta_0)P_{\eta_0,\pm\sigma}(v-\mu t,t|0,0). \tag{22}$$

Together with Eq. (12), the nth-order interval distribution is then given by the following sum over initial and final noise states:

$$J_{\mathrm{D},n}(T_n) = \sum_{\eta_0,\eta}(\mu+\eta)P_{\eta_0\eta}(nv_T-\mu T_n, T_n|0,0)p_F(\eta_0). \tag{23}$$

When plugging the probability densities Eqs. (20) and (21) into this expression, we finally obtain

$$J_{\mathrm{D},n}(T_n) = \frac{v_T\,\lambda^2}{\sigma\,\nu}\,\exp\{-\lambda\,[T_n - u\,(nv_T - \mu T_n)/\sigma]\} \times \left[\frac{\sigma}{\lambda}\left(\frac{1+u}{\mu-\sigma}\delta(T_n - T_n^+) + \frac{1-u}{\mu+\sigma}\,\delta(T_n - T_n^-)\right) + \left(\frac{n\nu}{2}\left[1 + \frac{\mu}{\mu+u\sigma}\left(1+\frac{\mu u}{\sigma}\right)\right] - \lambda T_n\left[1+\frac{\mu u}{\sigma}\right]\right)\frac{I_1[\alpha(T_n)/\gamma]}{\gamma\,\alpha(T_n)} + \frac{I_0[\alpha(T_n)/\gamma]}{\gamma^2}\right], \tag{24}$$

with $\alpha(T_n) = \lambda/\sigma\sqrt{\sigma^2 T_n^2 - (nv_T - \mu T_n)^2}$. This equation for the nth-order interval is valid for $T_n^+ \leqslant T_n \leqslant T_n^-$ with $T_n^\pm = \frac{nv_T}{\mu\pm\sigma}$. The nth-order interval density is zero for shorter and longer times T_n. To shorten notation, we have introduced the parameter

$$\nu = \frac{2\lambda v_T(\mu + u\sigma)}{\mu^2 - \sigma^2}. \tag{25}$$

If $u = 0$, Eq. (24) reduces to the expression found in [16].

Although we assumed $\sigma < \mu$ for our calculations, it is possible to take the limit $\sigma \to \mu$ in the expression for the ISI density [Eq. (24)]. In this case, the increase of the voltage is zero when the dichotomous noise is in the minus state. Thus, the threshold is always reached in the plus state. The limit yields an expression in which the second δ peak and the term proportional to I_0 vanish.

In the following, we discuss the obtained result and compare it with numerical simulations. Because higher-order distributions do not differ qualitatively, we restrict ourselves to the illustration of the ISI distribution (corresponding to the first-order interval, i.e., $n = 1$). Figure 4 displays the ISI distribution [Eq. (24)] for different mean transition rates. The distribution consists of two δ peaks and a continuous part; in a binned version of the histogram as shown in Fig. 4, the δ peaks turn into peaks of finite height while the continuous contribution changes only a little. The δ peaks correspond to realizations of the dichotomous noise in which no switching between noise states occurs while the voltage rises from the reset to the threshold. A short calculation shows that these peaks are weighted with the exponential factor $p_F(\pm\sigma)e^{-\lambda_\pm T_n^\pm}$. Hence, the distribution is clearly bimodal if the transition rates are small ($\lambda < 1$) and the asymmetry is not pronounced ($|u| < 1/2$). In the case of high transition rates, the exponential weights become so small that only a negligible fraction of the total probability is contained in the δ peaks. The continuous part becomes more and more peaked around the mean with increasing transition rates. In the limit of high transition rates, the distribution approaches an inverse Gaussian. This corresponds to the ISI distribution if Gaussian white noise drives the model (see below).

Figure 5 illustrates how the asymmetry u changes the ISI distribution: We see that a positive asymmetry shifts the peak of the distribution to shorter ISIs and makes it more pointed. This results from an increase in the mean input of the neuron model. A negative asymmetry has the contrary effect. Additionally, the asymmetry increases the probability contained in one of the δ peaks while reducing it in the other. Thus, a pronounced asymmetry leads to a more skewed distribution.

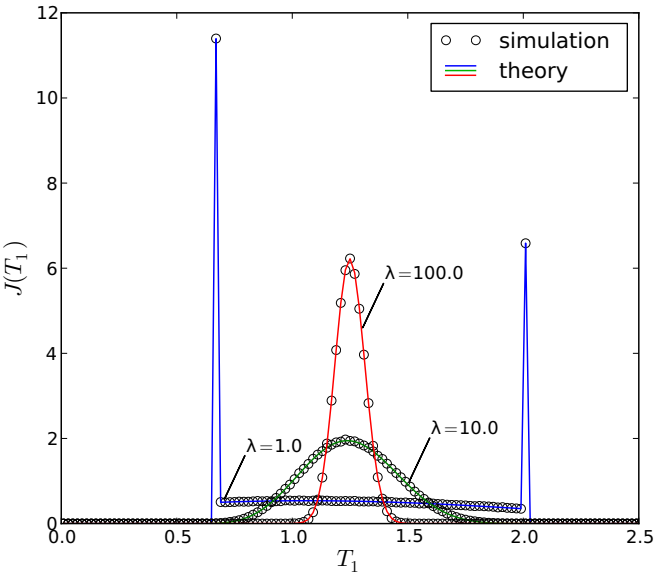

FIG. 4. (Color online) ISI distribution for different mean transition rates λ and dichotomous input only ($D = 0$). The theory (solid lines) is compared to stochastic simulations (black circles). Note that we use a temporally discretized histogram version of Eq. (24) (bin width equal to that of simulation data), in which δ peaks turn into peaks of finite height. Parameters: $\mu = v_T = 1.0, u = -0.4, \sigma = 0.5$.

To focus only on the effect of asymmetry, we compare ISI distributions with different u while keeping the mean and variance of the total input constant. Figure 6 shows that the asymmetry of the noise changes the asymmetry of the ISI distribution. The latter becomes more skewed to one direction.

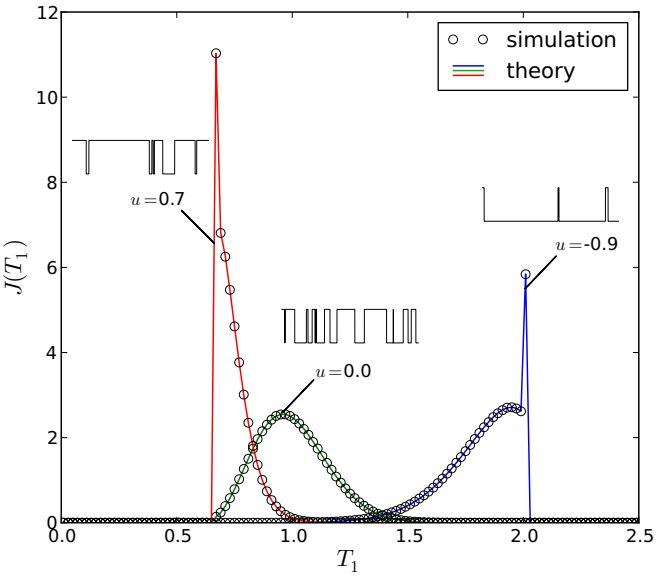

FIG. 5. (Color online) As Fig. 4 but for different asymmetries u and a mean transition rate $\lambda = 10$. When holding μ constant, a decreasing asymmetry shifts the distribution to the right.

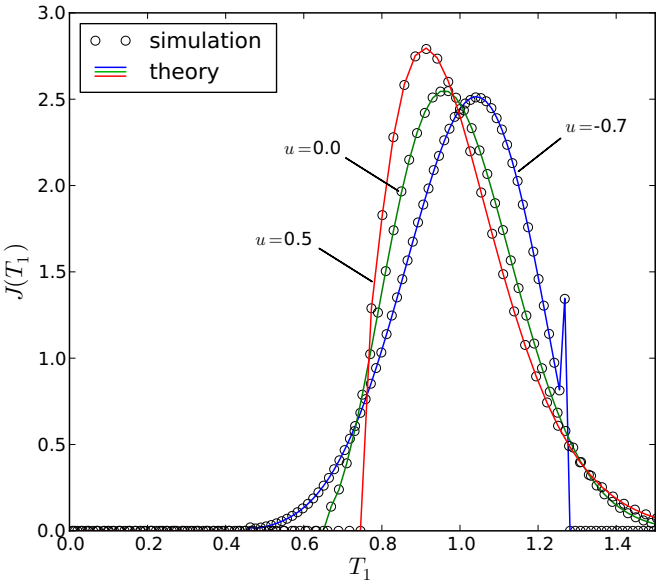

FIG. 6. (Color online) ISI distribution for different asymmetries u and a mean transition rate $\lambda = 10$. To illustrate only the effect of the asymmetry, we keep the mean and the variance of the input current constant: $\mu + u\sigma = 1$ and $\sigma^2(1-u^2) = 0.25$.

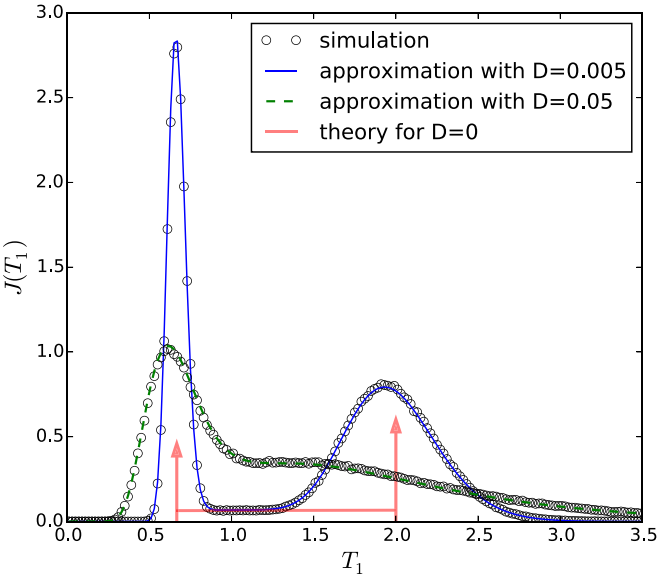

FIG. 7. (Color online) ISI distribution for a PIF neuron driven by Gaussian white noise and dichotomous noise. Stochastic simulation results (black circles) are compared to the approximation of Eq. (27). The δ peaks broaden with increasing noise intensity D. The plot shows examples for $D = 0.005$ and 0.05 and the model parameters $\lambda = 0.1$, $\mu = v_T = 1.0$, $\sigma = 0.5$, and $u = -0.6$.

In the next section, we quantify this effect by the skewness parameter of the ISI density.

Let us consider how the probability density of the nth-order interval changes as we include additional white noise input [$D > 0$ in Eq. (1)]. At the level of the density equation, this leads to additional second-order derivatives of $P_+(v,t)$ and $P_-(v,t)$ in Eqs. (10) and (11) as well as to a different boundary condition. An exact solution of this much more complicated problem (if possible at all) is beyond the scope of this paper, so we only discuss in the following an approximation of the nth-order interval density denoted by $J_{\mathrm{W+D},n}(T)$.

Our approximation is based on the assumption that the effects of the dichotomous noise and the white noise are separable, which should be valid for weak white noise and slow dichotomous driving. If the PIF model is driven by Gaussian white noise only, the solution for the probability density of the nth-order interval is equivalent to the first-passage-time density of an overdamped Brownian particle in a heat bath and subject to a constant force, which was solved by Schrödinger [38] and discussed in the neurobiological context by Gerstein and Mandelbrot [30]. The solution is given by the so-called inverse Gaussian distribution with mean nth-order interval $\bar{T}_n = nv_T/\mu$ and variance $2Dnv_T/\mu^3$,

$$J_{\mathrm{W},n}(t,\bar{T}_n) = \frac{nv_T}{\sqrt{4\pi Dt^3}} \exp\left(-\frac{(nv_T)^2(t-\bar{T}_n)^2}{4D\bar{T}_n^2 t}\right). \quad (26)$$

This formula also applies to our setup with both dichotomous and Gaussian noise if the dichotomous noise remains constant during the entire nth-order interval; the state of the dichotomous noise controls then the value of $\bar{T}_n$ but does not change the variance of the interval. For a very slow switching between the two states, the probability density could be approximated by a weighted sum of the two contribution corresponding to $\pm\sigma$ leading to the respective extremal intervals $\bar{T}_n = T_n^{\pm} = nv_T/(\mu \pm \sigma)$. The weight factors are exactly given by the probability density of the ISI in the absence of white noise, i.e., the prefactors of the δ functions in $J_{\mathrm{D},n}(T)$. Generalizing the idea of the weighted sum also to intervals in between the limits leads us to the following integral formula for the probability density of the nth-order interval in the presence of both dichotomous and Gaussian white noise,

$$J_{\mathrm{W+D},n}(T_n) = \int_0^\infty J_{\mathrm{W},n}(T_n,\bar{T}_n) J_{\mathrm{D},n}(\bar{T}_n) d\bar{T}_n. \quad (27)$$

By definition, this approximation is positive for every $T_n > 0$ and normalized to 1. The integral cannot be solved analytically, but numerical integration shows that the ISI density actually approximates the results of stochastic simulations very well if the mean transition rate λ is small. Figure 7 shows the approximation for a specific choice of parameters and compares it to the driving with dichotomous noise only. The δ peaks of the distribution without white noise broaden into inverse-Gaussian-shaped peaks. The continuous part of the distribution remains at the same height when adding weak white noise ($D = 0.005$). With stronger additional white noise ($D = 0.05$), both peaks show an increasing overlap such that the distribution loses its bimodal nature. For transition rates λ in the order of 1 or larger, there are significant deviations of the approximation from the simulations (not shown). We note that in both limit cases $\lambda \to \infty$ and $\lambda \to 0$, our approximation for the nth-order interval density Eq. (27) becomes exact.

IV. MOMENTS OF THE ISI DISTRIBUTION AND ISI CORRELATIONS

In this section, we derive the moments of the nth-order ISI distribution and use them to calculate the mean, variance,

and skewness γ_s of the ISI. Furthermore, we derive an expression for the serial correlation coefficient. Again, we start by considering dichotomous input only.

In principle, for $D = 0$ the ISI moments can be calculated by integrals over the probability density Eq. (24). However, the Bessel functions in this formula are difficult to integrate analytically. Therefore, we derive the moments of the distribution from its Laplace transform,

$$\hat{J}(v,s) = \int_0^\infty e^{-st} J(v,t)dt. \tag{28}$$

We recall that (i) the nth-order interval distribution is equivalent to the probability current Eq. (12) at $v = nv_T$; (ii) P_+ and P_- are solutions of the master equation (16). Because $J(v,t)$ is just a weighted sum of P_+ and P_-, $J(v,t)$ is a solution of Eq. (16) too. We can derive the following ordinary differential equation of second order by Laplace transforming the master equation:

$$\hat{J}'' + 2A\hat{J}' + B\hat{J} = C\delta(v) + \delta'(v), \tag{29}$$

where we have used the initial condition for the current,

$$J(v,0) = [(\mu+\sigma)p_F(\sigma) + (\mu-\sigma)p_F(\sigma)]\delta(v). \tag{30}$$

In Eq. (29), the prime denotes the derivative with respect to v. A, B, and C are functions of the Laplace transformed variable s:

$$A(s) = \frac{\lambda(\mu+u\sigma)+\mu s}{\mu^2-\sigma^2}, \quad B(s) = \frac{s(s+2\lambda)}{\mu^2-\sigma^2},$$
$$C(s) = \frac{2\lambda(\mu+u\sigma)}{\mu^2-\sigma^2} + \frac{s(\mu^2+\sigma^2+2\mu u\sigma)}{(\mu+u\sigma)(\mu^2-\sigma^2)}. \tag{31}$$

Equation (29) is solvable by standard methods. Requiring that $\hat{J}(v<0) = 0$ and $\hat{J}'(v<0) = 0$ fixes the integration constants. The final solution reads

$$\hat{J}(v,s) = e^{-v(A+\sqrt{A^2-B})}\left(\frac{1}{2} - \frac{C-A}{2\sqrt{A^2-B}}\right)\theta(v)$$
$$+ e^{-v(A-\sqrt{A^2-B})}\left(\frac{1}{2} + \frac{C-A}{2\sqrt{A^2-B}}\right)\theta(v). \tag{32}$$

From this expression, we can derive the kth moment of the ISI distribution by using the following property of the Laplace transform:

$$\langle T_n^k\rangle = (-1)^k \frac{\partial^k}{\partial s^k}\hat{J}(nv_T,s)\Big|_{s=0}. \tag{33}$$

Simplification of the formula for $k = 1,2,3$ leads to explicit expressions for the mean, the variance, and the third central moment:

$$\langle T_n\rangle = \frac{nv_T}{\mu+u\sigma}, \tag{34}$$

$$\langle \Delta T_n^2\rangle = \langle T_n^2\rangle - \langle T_n\rangle^2$$
$$= \frac{nv_T\sigma^2(1-u^2)}{\lambda(\mu+u\sigma)^3}\left[\frac{e^{-\nu n}-1}{\nu n}+1\right], \tag{35}$$

$$\langle \Delta T_n^3\rangle = \langle T_n^3\rangle - 3\langle T_n\rangle\langle \Delta T_n^2\rangle - \langle T_n\rangle^3$$
$$= \frac{3nv_T\sigma^2(1-u^2)(\sigma^2+\mu u\sigma)}{\lambda^2(\mu+u\sigma)^5}$$
$$\times\left[\frac{2}{\nu n}(e^{-\nu n}-1)+e^{-\nu n}+1\right]. \tag{36}$$

From these expressions, we can derive other statistical measures of the neuron model, such as the stationary firing rate r_0 and the coefficient of variation c_v:

$$r_0 = \frac{1}{\langle T_1\rangle} = \frac{\mu+u\sigma}{v_T}, \tag{37}$$

$$c_v = \frac{\sqrt{\langle \Delta T_1^2\rangle}}{\langle T_1\rangle} = \sqrt{\frac{\sigma^2(1-u^2)}{\lambda v_T(\mu+u\sigma)}\left[\frac{e^{-\nu}-1}{\nu}+1\right]}. \tag{38}$$

A shape measure that quantifies the asymmetry of the ISI distribution is the skewness γ_s. It is given by

$$\gamma_s = \frac{\langle \Delta T_1^3\rangle}{\langle \Delta T_1^2\rangle^{3/2}}. \tag{39}$$

Figure 8 illustrates how a varying asymmetry u of the dichotomous input changes the asymmetry of the ISI distribution. In the plot, we hold the mean and variance of the input constant while changing u. Because the theory requires $\mu > \sigma$, there is a maximal u for which this condition still holds if we keep the mean and variance constant. Figure 8 shows the monotonic increase in the skewness with increasing u. Furthermore, we can see that the skewness is more pronounced for small mean transition rates λ than for large ones.

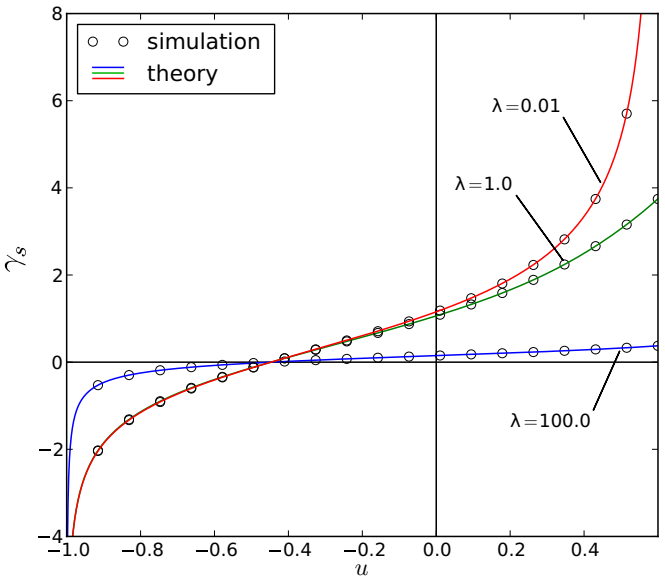

FIG. 8. (Color online) Skewness of the ISI distribution γ_s as a function of the asymmetry u of the dichotomous noise. The theory (colored lines) is compared to simulations (black circles) for different λ. u is varied while holding the mean $\mu+u\sigma = 1$ and the variance $\sigma^2(1-u^2) = 0.25$ of the input constant. Note that there is an upper limit for u because of the constraint of the theory $\mu > \sigma$.

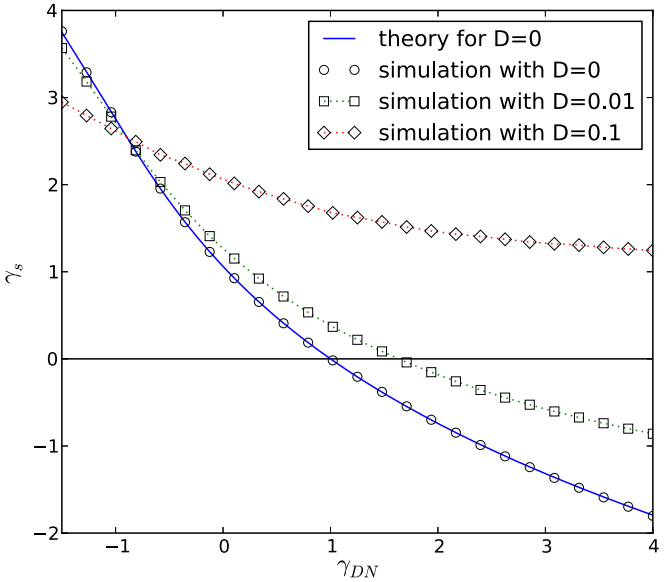

FIG. 9. (Color online) Skewness of the ISI distribution γ_s as a function of the input skewness γ_{DN} and the effect of additional white noise on it (theory, continuous line; simulations, black circles for $D = 0$; black squares, otherwise). The mean $\mu + u\sigma = 1$ and the variance $\sigma^2(1 - u^2) = 0.25$ of the input are kept constant. The theory requires $\mu > \sigma$, which results in a minimal input skewness.

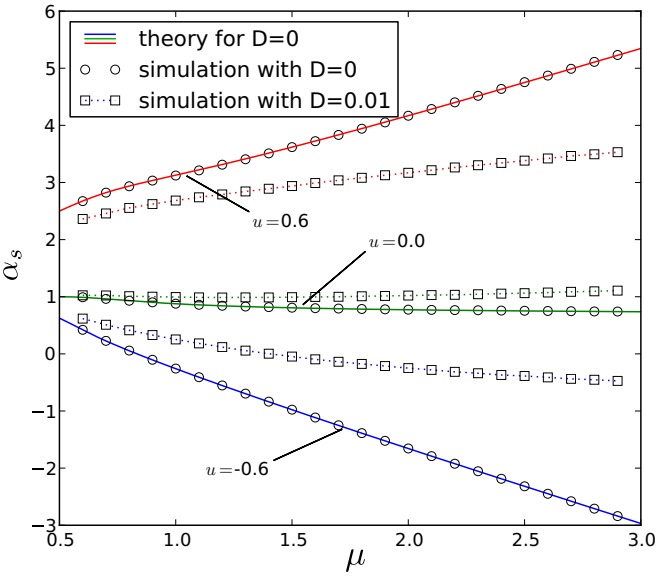

FIG. 10. (Color online) The rescaled skewness α_s plotted over the constant input current μ for different values of the noise asymmetry u. The black circles indicate simulations without white noise, which are in perfect agreement with the theory. The black squares are simulations with additional white noise $D = 0.01$. Remaining parameters: $\lambda = v_T = 1.0$, $\sigma = 0.5$.

A comparison to the skewness of the ISI distribution of a PIF neuron driven by Gaussian white noise with equivalent noise intensity $D = D_{\mathrm{DN}}$,

$$\gamma_s^{\mathrm{WN}} = 3\sqrt{\frac{2D}{\mu v_T}}, \tag{40}$$

reveals that for $u = 0$, γ_s is always smaller than γ_s^{WN} (not shown). With higher mean transition rates λ, the skewness approaches this value even for $u \neq 0$ because the slope of the u dependence becomes smaller. From Eqs. (35) and (36) it can be shown that the skewness diverges to $\pm\infty$ in the limits $u \to \pm 1$.

To plot the relationship between the asymmetries of the dichotomous input and of the resulting ISI distribution differently, we can relate u to the skewness of the dichotomous noise γ_{DN} via Eq. (5). Figure 9 illustrates the dependence of the skewness of the ISI distribution on the skewness of the dichotomous input. This time, there is a minimal value corresponding to the constraint that $\mu > \sigma$. Clearly, the ISI skewness decreases monotonically with the skewness of the noise. A bias toward smaller (larger) values of the dichotomous process is associated with a positive (negative) skewness of the input noise and leads to a preference of longer (shorter) ISIs, which in turn results in a negative (positive) ISI skewness. Figure 9 also demonstrates the effect of additional white noise. In general, additional Gaussian white noise decreases the slope of the function but does not change the monotonic decline of the ISI skewness with increasing noise skewness. The change in slope is more pronounced for the larger noise intensity.

To capture deviations of the skewness from a PIF model driven only by white noise, we rescale the skewness such that it is 1 for an inverse Gaussian. The skewness of an inverse Gaussian is equal to $3c_v$, so that the rescaled skewness α_s is defined as [39]

$$\alpha_s = \frac{\gamma_s}{3c_v} = \frac{\langle \Delta T^3 \rangle \langle T \rangle}{3\langle \Delta T^2 \rangle^2}. \tag{41}$$

In the absence of white noise, we can compute α_s from Eqs. (34)–(36). Figure 10 shows the change in the rescaled skewness α_s with increasing base current μ. The increase or decrease in α_s at large values of μ is directly related to the asymmetry u. In the limit of large μ, the curve approaches the asymptotic straight line,

$$\alpha_s \approx \frac{2\lambda u \sigma v_T + 3\sigma^2}{9\sigma^2(1-u^2)} + \frac{2u}{\sigma^2(1-u^2)}\mu. \tag{42}$$

In some parameter regimes, however, α_s shows a nonmonotonic dependency on μ at small values μ (not shown). Although additional white noise diminishes the effect of dichotomous noise on the skewness (cf. squares in Fig. 10), the qualitative dependence remains the same even for $D > 0$.

In an experiment, one could inject a constant current into a cortical cell receiving input from a presynaptic population showing up-down states. This corresponds to a change in the parameter μ of the model. A monotonic change in the rescaled skewness then may indicate an asymmetry in the presynaptic input.

We now turn to the calculation of the serial correlation coefficient ρ_k for the output spike train. To do so, we make use of the following relation between the variance of the nth-order interval $\mathrm{var}(T_n)$ and the SCC [16]:

$$\rho_k = \frac{\mathrm{var}(T_{k-1}) + \mathrm{var}(T_{k-1}) - 2\,\mathrm{var}(T_k)}{2\,\mathrm{var}(T_1)}. \tag{43}$$

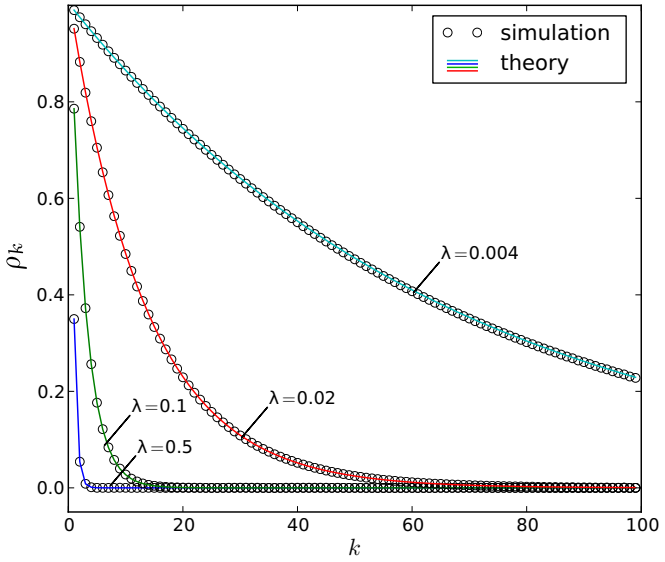

FIG. 11. (Color online) Serial correlation coefficient obtained by simulations (black circles) compared with the theory (colored lines) for pure dichotomous noise ($D = 0$) [Eq. (44)]. The curves show the SCC for different mean transition rates λ. Remaining model parameters: $\mu = v_T = 1.0$, $\sigma = 0.5$, and $u = 0.8$.

Using the variance Eq. (35), Eq. (43) yields, after some simplifications, a simple expression for the SCC,

$$\rho_k = \frac{2\sinh^2(\nu/2)}{\nu - 1 + e^{-\nu}} e^{-k\nu}. \tag{44}$$

This expression has the same form as the SCC for symmetric dichotomous noise found in [16]. The only difference is that the asymmetry u appears in the parameter ν [cf. Eq. (25)]. Figure 11 shows that the theory agrees with numerical simulations. In the limit $\sigma \to \mu$ discussed above, ν goes to infinity and thus the correlations become zero. This result agrees with the consideration that the noise cannot carry memory from one ISI to the next if the threshold is only reached in one of the two noise states [40].

To obtain an approximation for the ISI correlations in the case of driving with both dichotomous and Gaussian white noise, we can make use of the approximation discussed in the preceding section. Additional white noise decreases the correlations. Because all correlations result from the dichotomous noise, it is reasonable to assume that the major contribution to the expected decorrelation comes from an increased variance in the denominator of Eq. (43). The approximation Eq. (27) allows us to calculate the increase of the variance due to additional white noise to linear order in D:

$$\mathrm{var}(T_{\mathrm{DN+WN}}) \approx \langle \Delta T_{\mathrm{DN}}^2 \rangle + \frac{2D}{v_T^2} \langle T_{\mathrm{DN}}^3 \rangle, \tag{45}$$

where $\langle T_{\mathrm{DN}}^3 \rangle$ is the third moment of the ISI distribution with only dichotomous noise given in Eq. (36). Using this approximation, we obtain the following expression for the serial correlation coefficient:

$$\rho_k^{\mathrm{DN+WN}} \approx \frac{\rho_k^{\mathrm{DN}}}{1 + \beta D}, \quad \beta = \frac{2\langle T_{\mathrm{DN}}^3 \rangle}{v_T^2 \langle \Delta T_{\mathrm{DN}}^2 \rangle}. \tag{46}$$

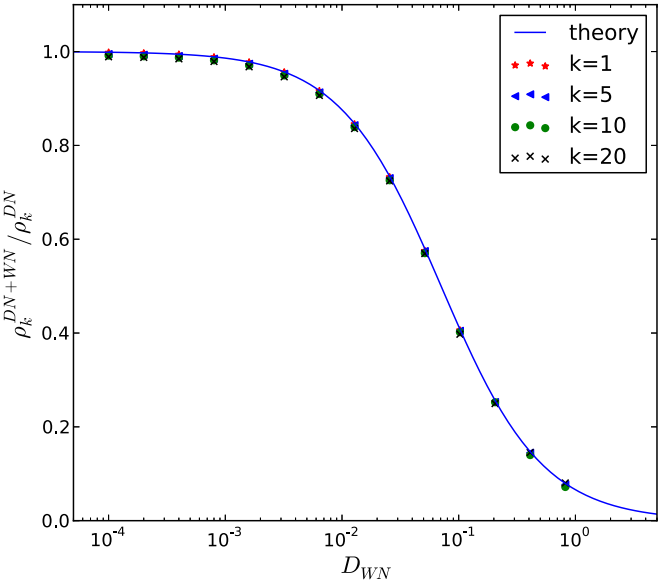

FIG. 12. (Color online) Serial correlation coefficients (for lag $k = 1$, 5, 10, and 20) normalized by the respective SCC without white noise and plotted over different white noise intensities. The dots represent stochastic simulations, whereas the solid line shows the approximation of Eq. (46) with model parameters $\lambda = 0.01$, $\mu = v_T = 1.0$, $\sigma = 0.5$, and $u = 0.6$.

Numerical simulations (Fig. 12) at small switching rates confirm the prediction of the correlation reduction by white noise quantitatively. In particular, the reduction seems to be independent of the lag k: Fig. 12 shows the SCC for different lags k normalized by the respective SCC without white noise, resulting in data points that are on top of each other and agree well with the theoretical formula. The figure further suggests that, at least for strong ISI correlations induced by a slow dichotomous noise, the approximation is valid for quite large noise intensities D.

V. POWER SPECTRUM

We now turn to the calculation of a second-order spike-train statistics, the power spectrum of $x(t)$. The starting point of our consideration is the correlation function $C(\tau) = \langle x(t)x(t+\tau)\rangle - \langle x(t)\rangle^2$, which can be expressed [41] by $C(\tau) = r_0[\delta(\tau) + m(\tau)] - r_0^2$. Here r_0 is the stationary firing rate and $m(\tau)$ denotes the spike-triggered rate, i.e., the conditional probability density to observe a spike at time $t + \tau$ given that there was (another) spike at time t. The power spectrum, defined in Eq. (9), is related to the correlation function by a Fourier transformation (Wiener-Khinchin theorem), and hence it follows that [7,41,42]

$$S(\omega) = r_0(1 + 2\,\mathrm{Re}(\widetilde{m}(\omega))), \tag{47}$$

with the stationary firing rate r_0 and the one-sided Fourier transform of the spike-triggered rate

$$\widetilde{m}(\omega) = \int_0^\infty e^{i\omega t} m(t) dt. \tag{48}$$

This quantity is the transform of a real valued function and thus obeys $\widetilde{m}^*(\omega) = \widetilde{m}(-\omega)$. In the following, we mark all

quantities that are one-sided Fourier transforms with a tilde. For a shorter notation, we use angular frequencies ω, which readily transform to normal frequencies $f = \omega/(2\pi)$.

In principle, we know $m(t)$ already and could calculate the spectrum from Eqs. (48) and (47): the spike-triggered rate is given by the sum over all nth-order interval densities [7]

$$m(t) = \sum_{n=1}^{\infty} J_{\mathrm{D},n}(t). \tag{49}$$

However, the summation over the Bessel functions and the Fourier transformation of the result are difficult. Here we use another method, which is based on the Fourier transformation of the master equations and is similar to the method outlined in Ref. [42] for the case of a white-noise-driven IF model.

To calculate $\widetilde{m}(\omega)$ for the case of purely dichotomous noise, we start with the master equations (10) and (11). To capture all spikes and not only the first spike, we have to include terms that describe the absorption and reset of the voltage trajectory,

$$\partial_t P_+ = \lambda_- P_- - \lambda_+ P_+ - (\mu+\sigma)\partial_v P_+ + m_+(t) f(v), \tag{50}$$

$$\partial_t P_- = \lambda_+ P_+ - \lambda_- P_- - (\mu-\sigma)\partial_v P_- + m_-(t) f(v), \tag{51}$$

with $f(v) = \delta(v) - \delta(v - v_T)$. Here, we have split $m(t) = m_+(t) + m_-(t)$ into two parts, $m_+(t)$ and $m_-(t)$, corresponding to spikes that occur during the plus and minus states, respectively. Both functions are not yet known (in fact, our consideration only serves the purpose of calculating them), but their Fourier transforms can be found as outlined in the following. Initial conditions for Eqs. (50) and (51) are as above for the first-passage-time problem, i.e., $P_\pm(v,0) = p_F(\pm\sigma)\delta(v)$.

From the master equations (50) and (51), we can obtain a second-order partial differential equation for $P_\pm$ with the same homogeneous part as Eq. (16). By virtue of the equation's linearity, we may instead write the same type of equation for the total probability current J defined in Eq. (12) and for the difference between the currents in the plus and in the minus state,

$$Q = (\mu+\sigma)P_+ - (\mu-\sigma)P_-. \tag{52}$$

To determine the two quantities $\widetilde{m}_+$ and $\widetilde{m}_-$, we need to compute the Fourier transforms of the two functions J and Q. To do so, we perform a one-sided Fourier transformation of the resulting differential equations for J and Q, which reduces them to simpler ordinary differential equations:

$$\widetilde{L}_0 \widetilde{J} = h_j^- \widetilde{m}_- + h_j^+ \widetilde{m}_+ + h_j^i, \tag{53}$$

$$\widetilde{L}_0 \widetilde{Q} = h_q^- \widetilde{m}_- + h_q^+ \widetilde{m}_+ + h_q^i, \tag{54}$$

where $\widetilde{J}$ and $\widetilde{Q}$ as well as the inhomogeneities h are functions of ω and v, and $\widetilde{L}_0$ denotes the Fourier transform of the operator of the resulting homogeneous equation,

$$\widetilde{L}_0 = \frac{d^2}{dv^2} + 2A(\omega)\frac{d}{dv} + B(\omega), \tag{55}$$

with

$$A(\omega) = \frac{\lambda(\mu+u\sigma) - i\omega\mu}{\mu^2-\sigma^2}, \quad B(\omega) = -\frac{\omega^2 + 2i\omega\lambda}{\mu^2-\sigma^2}. \tag{56}$$

The inhomogeneities resulting from absorption and reset ($h^\pm$) and from the initial conditions (h^i) are given by

$$h_j^\pm = C_j^\pm(\omega) f(v) + f'(v), \tag{57}$$

$$h_j^i = C_j^i(\omega)\delta(v) + \delta'(v), \tag{58}$$

$$h_q^\pm = C_q^\pm(\omega) f(v) + f'(v), \tag{59}$$

$$h_q^i = C_q^i(\omega)\delta(v) + D_q^i \delta'(v), \tag{60}$$

with the coefficients

$$C_j^+(\omega) = \frac{-i\omega(\mu+\sigma) + 2\lambda(\mu+u\sigma)}{\mu^2-\sigma^2}, \tag{61}$$

$$C_j^-(\omega) = \frac{-i\omega(\mu-\sigma) + 2\lambda(\mu+u\sigma)}{\mu^2-\sigma^2}, \tag{62}$$

$$C_j^i(\omega) = \frac{2\lambda(\mu+u\sigma) - \frac{i\omega}{\mu+u\sigma}(\mu^2+\sigma^2+2\mu u\sigma)}{\mu^2-\sigma^2}, \tag{63}$$

$$C_q^+(\omega) = \frac{-i\omega(\mu+\sigma) + 2\lambda\sigma\left(1+\frac{\mu u}{\sigma}\right)}{\mu^2-\sigma^2}, \tag{64}$$

$$C_q^-(\omega) = \frac{i\omega(\mu-\sigma) + 2\lambda\sigma\left(1+\frac{\mu u}{\sigma}\right)}{\mu^2-\sigma^2}, \tag{65}$$

$$C_q^i(\omega) = \frac{2\lambda\sigma\left(1+\frac{\mu u}{\sigma}\right) - \frac{i\omega}{\mu+u\sigma}[2\mu\sigma + u(\mu^2+\sigma^2)]}{\mu^2-\sigma^2}, \tag{66}$$

$$D_q^i = \frac{\sigma}{\mu+u\sigma}\left(1+\frac{\mu u}{\sigma}\right). \tag{67}$$

Because Eqs. (53) and (54) are linear, we can construct the full solutions from the solutions for only one inhomogeneity. Specifically, $\widetilde{J}$ and $\widetilde{Q}$ can be expressed as the sums

$$\widetilde{J} = \widetilde{m}_- \widetilde{J}^- + \widetilde{m}_+ \widetilde{J}^+ + \widetilde{J}^i, \tag{68}$$

$$\widetilde{Q} = \widetilde{m}_- \widetilde{Q}^- + \widetilde{m}_+ \widetilde{Q}^+ + \widetilde{Q}^i, \tag{69}$$

where $\widetilde{J}^k$ and $\widetilde{Q}^k$ are solutions of

$$\widetilde{L}_0 \widetilde{J}^k = h_j^k, \tag{70}$$

$$\widetilde{L}_0 \widetilde{Q}^k = h_q^k, \tag{71}$$

with $k = +, -, i$. We obtain them with standard methods by using the conditions $J^k(v<0,\omega)$ and $Q^k(v<0,\omega) = 0$. For the inhomogeneities from the initial conditions, the solutions are

$$J^i(v,\omega) = \theta(v) e^{-vA(\omega)} \times \left[\cosh[vF(\omega)] + \frac{C_j^i(\omega) - A(\omega)}{F(\omega)}\sinh[vF(\omega)]\right], \tag{72}$$

$$Q^i(v,\omega) = \theta(v)e^{-vA(\omega)}\Big[D_q^i \cosh[vF(\omega)] + \frac{C_q^i(\omega) - D_q^i A(\omega)}{F(\omega)} \sinh[vF(\omega)]\Big], \quad (73)$$

with

$$F(\omega) = \sqrt{A(\omega)^2 - B(\omega)} = \frac{\sqrt{\lambda^2(\mu + u\sigma)^2 - 2i\omega\lambda\sigma(\sigma + \mu u) - \sigma^2\omega^2}}{\mu^2 - \sigma^2} \quad (74)$$

[$A(\omega)$ and $B(\omega)$ were defined in Eq. (56)]. The differential equations with inhomogeneities from absorption and reset yield

$$\widetilde{J}^{\pm}(v,\omega) = \left(\frac{1}{2} - \frac{C_j^{\pm}(\omega) - A(\omega)}{2F(\omega)}\right)\varphi_+(v) + \left(\frac{1}{2} + \frac{C_j^{\pm}(\omega) - A(\omega)}{2F(\omega)}\right)\varphi_-(v), \quad (75)$$

$$\widetilde{Q}^{\pm}(v,\omega) = \left(\frac{1}{2} - \frac{C_q^{\pm}(\omega) - A(\omega)}{2F(\omega)}\right)\varphi_+(v) + \left(\frac{1}{2} + \frac{C_q^{\pm}(\omega) - A(\omega)}{2F(\omega)}\right)\varphi_-(v), \quad (76)$$

where

$$\varphi_{\pm}(v) = \theta(v)e^{-v[A(\omega)\pm F(\omega)]} - \theta(v - v_T)e^{-(v-v_T)[A(\omega)\pm F(\omega)]}. \quad (77)$$

Our aim is to calculate the Fourier transforms of the spike-triggered rate $\widetilde{m} = \widetilde{m}_+ + \widetilde{m}_-$. To do so, we can use the boundary condition that $\widetilde{J}$ and $\widetilde{Q}$ have to vanish for $v > v_T$ because all voltage trajectories are reset when they reach v_T. This condition allows us to determine the spike-triggered rates:

$$\widetilde{m}_+ = \frac{\widetilde{J}^i\widetilde{Q}^- - \widetilde{J}^-\widetilde{Q}^i}{\widetilde{J}^-\widetilde{Q}^+ - \widetilde{J}^+\widetilde{Q}^-}, \quad \widetilde{m}_- = \frac{\widetilde{J}^+\widetilde{Q}^i - \widetilde{J}^i\widetilde{Q}^+}{\widetilde{J}^-\widetilde{Q}^+ - \widetilde{J}^+\widetilde{Q}^-}, \quad (78)$$

where the different $\widetilde{J}$'s and $\widetilde{Q}$'s are all taken at $v > v_T$. In the expressions for $\widetilde{m}_-$ and $\widetilde{m}_+$, the v dependences cancel each other out.

Using the above expressions for $\widetilde{J}^k$ and $\widetilde{Q}^k$, we find, after substantial simplifications,

$$\widetilde{m}(\omega) = (2\{\cosh[v_T A(\omega)] - \cosh[v_T F(\omega)]\})^{-1} \times \left[\frac{A(\omega) + \frac{i\omega}{\mu + u\sigma}}{F(\omega)} \sinh[v_T F(\omega)] + \cosh[v_T F(\omega)] - e^{-v_T A(\omega)}\right]. \quad (79)$$

This is the final result of this section, and together with Eq. (47) it permits the calculation of the spike-train power spectrum. Note that in general, $F(\omega)$ is a complex-valued function, which as an argument of the hyperbolic functions introduces periodic components into the power spectrum.

Figure 13 shows examples of the spike-train power spectra of a PIF neuron with dichotomous driving and compares the analytical result to those of numerical simulation. In particular, at small values of the switching rate λ, the shape is rather unusual for a spike-train power spectrum (for some experimental examples of power spectra, see [43]): the spectrum has a clearly periodic part; in particular, this periodicity dominates at large frequencies. There are two characteristic frequencies and multiples thereof at which peaks occur in the spectrum,

$$\omega_{\pm} = 2\pi\frac{\mu \pm \sigma}{v_T}. \quad (80)$$

These frequencies correspond to the two values at which δ functions occur in the ISI distribution, i.e., the realizations where no switching occurs between reset and threshold. Mathematically, we can understand the occurrence of undamped oscillations in the power spectrum by looking at Eqs. (49) and (47). The power spectrum given in Eq. (47) contains the Fourier transform of a sum, Eq. (49), that contains δ peaks according to Eq. (24). The Fourier transform of a δ peak yields an undamped oscillation, which explains why we observe such unusual periodicity in the spectrum. For an alternative explanation, one may consider that the power spectrum of a Dirac comb (a perfectly regular spike train with random initial time) is again a Dirac comb [7], i.e., it exhibits undampened periodicity. The spike train of our model can be regarded as a sequence of time windows with perfectly regularly spaced spikes, i.e., finite-duration "Dirac combs." Because the durations of the time windows are stochastic, the resulting periodic structure in the power spectrum does not contain δ peaks as it would do for an infinite Dirac comb. Hence, the particular features of the power spectrum rely solely on the discrete support of the dichotomous noise.

At small transition rates λ, the ratio between the height of the two different peaks corresponds to the square of the ratio between the probabilities of crossing the threshold in one of

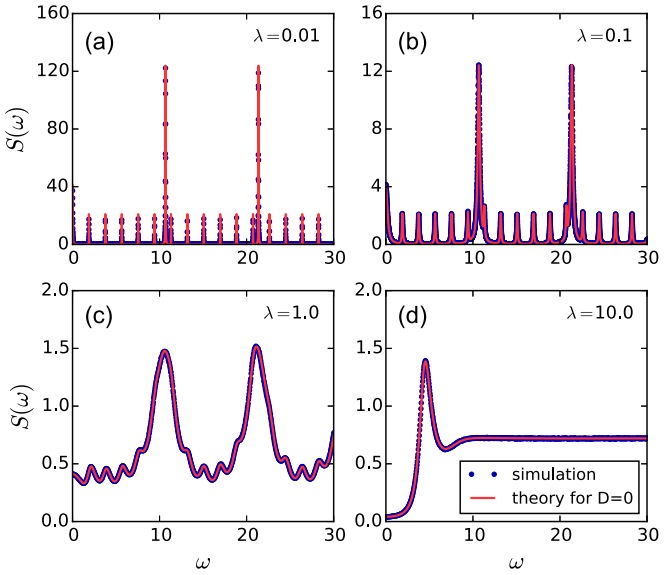

FIG. 13. (Color online) The power spectrum $S(\omega)$ from simulations (blue dots) compared with the theory [red (light gray) solid line], Eqs. (47) and (79), for different mean transition rates λ and purely dichotomous input. Remaining parameters: $\mu = v_T = 1.0$, $\sigma = 0.7$, $u = -0.4$.

the noise states. Thus, the relative peak height is influenced by the asymmetry of the driving process. With increasing λ, the peaks broaden until they overlap such that the spectrum is almost constant for high frequencies. However, even for high λ, there remains a small oscillating part, which is related to the survival of the δ peaks in the nth-order interval density for any finite value of λ. This behavior clearly differs from the power spectra of model neurons driven by white noise [44], where all oscillations vanish at high frequencies and the power spectrum approaches r_0. In fact, even if the input noise is colored but has a continuous support, we do not expect oscillations in the high-frequency part of the power spectrum, which is in line with previous results for a PIF neuron driven by an Ornstein-Uhlenbeck process [15].

The limit $\omega \to 0$ of the power spectrum is linked to the serial correlation coefficient by the general relation [45]

$$\lim_{\omega\to 0} S(\omega) = r_0 c_v^2 \left(1 + \sum_{k=1}^{\infty} \rho_k\right) = r_0 F_\infty, \tag{81}$$

where F_∞ is the Fano factor in the limit of large spike count windows. The Fano factor is defined as the variance over the mean of the spike count in a specified time window and thus is a relative measure of the count variability. Taking the limit as well as performing the infinite sum yield the same expression and thus shows that the results for the SCC and the power spectrum are consistent. The resulting Fano factor is given by the simple expression

$$F_\infty = \frac{\sigma^2(1-u^2)}{v_T\lambda(\mu + u\sigma)}. \tag{82}$$

Interestingly, this expression corresponds to the result for a PIF neuron driven by white noise, for which the Fano factor is given by $F_\infty = 2D/(v_T\mu)$. Here, one has to replace the white noise intensity D by the noise intensity of the dichotomous noise, $D_{\mathrm{DN}} = \tau_c\langle\Delta\eta(t)^2\rangle$.

How much of the peculiar spectral structure survives if the neuron is additionally driven by white noise? For the parameters from Fig. 13(b) we have inspected this by numerical simulations (Fig. 14). With increasing white noise, the spectral multipeaked structure is replaced by one with fewer and broader peaks. When driving the model neuron with both dichotomous and white noise, the periodicity of the power spectrum is damped toward high frequencies. In the limit $\omega \to \infty$, it saturates at the stationary firing rate. As Fig. 14 shows, the periodicity decays stronger with higher white noise intensities D and the peaks become wider. With $D = 0.1$ there is hardly any periodic structure left.

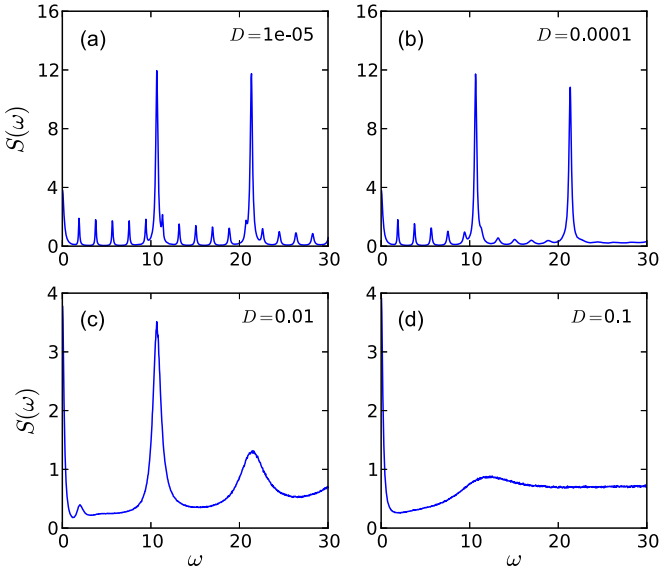

FIG. 14. (Color online) The simulated power spectrum $S(\omega)$ of a PIF neuron driven by dichotomous noise and Gaussian white noise for different white-noise intensities D as indicated. Remaining parameters as in Fig. 13(b).

VI. CONCLUSION

This paper explored the effect of correlations and asymmetry of neuronal input noise on the firing statistics of a single neuron. To get some analytical insights, we derived different spike-train statistics for a perfect integrate-and-fire neuron driven by asymmetric dichotomous noise: the ISI distribution, the serial correlation coefficient, and the power spectrum. We verified the analytical expressions with stochastic simulations. We found a set of features that stem from the noise correlations and the asymmetry in the dichotomous noise: In contrast to the statistics of a neuron driven by uncorrelated noise, the ISI distribution is clearly bimodal for small transition rates of the input noise. In the limit of high transition rates, the distribution approaches an inverse Gaussian. A high asymmetry between the rates of the dichotomous noise leads to a strongly skewed distribution of interspike intervals.

The ISI correlations decay exponentially with the lag, as previously found in [16] for symmetric dichotomous noise. In our case, both the decay constant and the prefactor are functions of the asymmetry, but asymmetric noise does not lead to qualitatively different behavior. The power spectrum shows periodic oscillations at high frequencies. In contrast to the driving with Gaussian noise, the oscillations do not decay at large frequencies.

We also gave approximations of the ISI statistics for a model neuron driven by both slow dichotomous and Gaussian white noise, which were confirmed by numerical simulations. Here we focused on the case of slow dichotomous noise because in this limit the effects of the non-Gaussian correlated noise process are most pronounced. We found that white noise decreases the positive ISI correlations caused by the dichotomous input by a factor independent of the lag. Furthermore, numerical simulations of the power spectra show that the periodic oscillations from the dichotomous noise are damped due to additional white noise.

The theory can possibly be applied in experimental studies of up-down states in the cortex. Because up-down states are collective phenomena of neural populations, their measurement requires a lot of experimental effort. The output statistics of a neuron may allow us to infer properties of this joint activity of a presynaptic neural population from the firing statistics of a neuron receiving such two-state-like input currents. For example, the ISI density can show features such as bimodality that hint at dichotomous input. Furthermore,

exponentially decaying ISI correlations are likely to stem from exponentially correlated input. By injecting constant input currents of varying amplitude, the rescaled skewness of the ISI distribution could allow us to infer information about the asymmetry of up-down state transitions via the parametric dependence shown in Fig. 10. One assumption that has to be met to apply our results in such investigations would be that the considered neuron is in a mean-driven (tonically spiking) regime, for which an approximation by a perfect IF model can be meaningful [18,31].

The neural dynamics of the perfect integrate-and-fire model is simple, but more elaborate models can show similar features. Preliminary simulation results (not shown) suggest that the results for the ISI distribution can approximate a leaky integrate-and-fire (LIF) model in the tonically firing regime with a small leak. By rescaling the parameters of the PIF model, we were able to approximate the ISI density of an LIF (for a similar method in the case of driving with white noise and adaptation current, see [46]). However, further analysis is needed to investigate which of the features of the spike statistics, analytically revealed in our study, are preserved in biophysically more realistic neuron models with a spike-generating mechanism.

ACKNOWLEDGMENTS

We acknowledge funding by the Bundesministerium für Bildung und Forschung (BMBF) (FKZ: 01GQ1001A) and the Deutsche Forschungsgemeinschaft (DFG) under the project Research Training Group GRK 1589/1.

[1] B. Lindner, J. Garcia-Ojalvo, A. Neiman, and L. Schimansky-Geier, Effects of noise in excitable systems, Phys. Rep. **392**, 321 (2004).
[2] P. Hänggi, Stochastic resonance in biology - How noise can enhance detection of weak signals and help improve biological information processing, Chem. Phys. Chem. **3**, 285 (2002).
[3] A. A. Faisal, L. P. J. Selen, and D. M. Wolpert, Noise in the nervous system, Nat. Rev. Neurosci. **9**, 292 (2008).
[4] G. B. Ermentrout, R. F. Galan, and N. N. Urban, Reliability, synchrony and noise, Trends Neurosci. **31**, 428 (2008).
[5] T. Branco and K. Staras, The probability of neurotransmitter release: Variability and feedback control at single synapses, Nat. Rev. Neurosci. **10**, 373 (2009).
[6] J. A. White, J. T. Rubinstein, and A. R. Kay, Channel noise in neurons, Trends Neurosci. **23**, 131 (2000).
[7] A. V. Holden, *Models of the Stochastic Activity of Neurones* (Springer, Berlin Heidelberg, 1976).
[8] H. C. Tuckwell, *Stochastic Processes in the Neurosciences* (SIAM, Philadelphia, PA, 1989), Vol. 56.
[9] A. N. Burkitt, A review of the integrate-and-fire neuron model: I. Homogeneous synaptic input, Biol. Cybern. **95**, 1 (2006).
[10] A. N. Burkitt, A review of the integrate-and-fire neuron model: II. Inhomogeneous synaptic input and network properties, Biol. Cybern. **95**, 97 (2006).
[11] N. Fourcaud and N. Brunel, Dynamics of the firing probability of noisy integrate-and-fire neurons, Neural Comput. **14**, 2057 (2002).
[12] N. Fourcaud-Trocmé, D. Hansel, C. Van Vreeswijk, and N. Brunel, How spike generation mechanisms determine the neuronal response to fluctuating inputs, J. Neurosci. **23**, 11628 (2003).
[13] R. Moreno, J. de la Rocha, A. Renart, and N. Parga, Response of spiking neurons to correlated inputs, Phys. Rev. Lett. **89**, 288101 (2002).
[14] N. Brunel and P. E. Latham, Firing rate of the noisy quadratic integrate-and-fire neuron, Neural Comput. **15**, 2281 (2003).
[15] J. W. Middleton, M. J. Chacron, B. Lindner, and A. Longtin, Firing statistics of a neuron model driven by long-range correlated noise, Phys. Rev. E **68**, 021920 (2003).
[16] B. Lindner, Interspike interval statistics of neurons driven by colored noise, Phys. Rev. E **69**, 022901 (2004).
[17] T. Schwalger and L. Schimansky-Geier, Interspike interval statistics of a leaky integrate-and-fire neuron driven by Gaussian noise with large correlation times, Phys. Rev. E **77**, 031914 (2008).
[18] C. Bauermeister, T. Schwalger, D. F. Russell, A. B. Neiman, and B. Lindner, Characteristic effects of stochastic oscillatory forcing on neural firing: Analytical theory and comparison to paddlefish electroreceptor data, PLoS Comput. Biol. **9**, e1003170 (2013).
[19] M. J. E. Richardson and W. Gerstner, Synaptic shot noise and conductance fluctuations affect the membrane voltage with equal significance, Neural Comput. **17**, 923 (2005).
[20] L. Wolff and B. Lindner, A method to calculate the moments of the membrane voltage in a model neuron driven by multiplicative filtered shot noise, Phys. Rev. E **77**, 041913 (2008).
[21] M. J. E. Richardson and R. Swarbrick, Firing-rate response of a neuron receiving excitatory and inhibitory synaptic shot noise, Phys. Rev. Lett. **105**, 178102 (2010).
[22] E. Salinas and T. J. Sejnowski, Integrate-and-fire neurons driven by correlated stochastic input, Neural Comput. **14**, 2111 (2002).
[23] F. Droste and B. Lindner, Integrate-and-fire neurons driven by asymmetric dichotomous noise, Biol. Cybern. **108**, 825 (2014).
[24] W. Horsthemke and R. Lefever, *Noise-Induced Transitions*, 2nd ed. (Springer, Berlin Heidelberg, 2006).
[25] C. Van Den Broeck, On the relationship between white shot noise, Gaussian white noise, and the dichotomic Markov process, J. Stat. Phys. **31**, 467 (1983).
[26] V. Balakrishnan, S. Lakshmibala, and C. Van Den Broeck, The renewal equation for persistent diffusion, Physica A **153**, 57 (1988).
[27] P. Hänggi and P. Jung, Colored noise in dynamical systems, Adv. Chem. Phys. **89**, 239 (1995).
[28] V. Balakrishnan and C. Van den Broeck, Solvability of the master equation for dichotomous flow, Phys. Rev. E **65**, 012101 (2001).
[29] I. Bena, Dichotomous Markov noise: Exact results for out-of-equilibrium systems, Int. J. Mod. Phys. B **20**, 2825 (2006).

[30] G. L. Gerstein and B. Mandelbrot, Random walk models for the spike activity of a single neuron, Biophys. J. **4**, 41 (1964).
[31] K. Fisch, T. Schwalger, B. Lindner, A. V. M. Herz, and J. Benda, Channel noise from both slow adaptation currents and fast currents is required to explain spike-response variability in a sensory neuron, J. Neurosci. **32**, 17332 (2012).
[32] R. L. Cowan and C. J. Wilson, Spontaneous firing patterns and axonal projections of single corticostriatal neurons in the rat medial agranular cortex, J. Neurophysiol. **71**, 17 (1994).
[33] Y. Shu, A. Hasenstaub, and D. A. McCormick, Turning on and off recurrent balanced cortical activity, Nature **423**, 288 (2003).
[34] A. Luczak, P. Bartho, S. L. Marguet, G. Buzsaki, and K. D. Harris, Sequential structure of neocortical spontaneous activity in vivo, Proc. Natl. Acad. Sci. USA **104**, 347 (2007).
[35] V. Balakrishnan and S. Chaturvedi, Persistent diffusion on a line, Physica A **148**, 581 (1988).
[36] V. Balakrishnan and S. Lakshmibala, On the connection between biased dichotomous diffusion and the one-dimensional Dirac equation, New J. Phys. **7**, 11 (2005).
[37] P. Morse and H. Feshbach, *Methods of Theoretical Physics* (McGraw-Hill, New York, 1953).
[38] E. Schrödinger, Zur Theorie der Fall- und Steigversuche an Teilchen mit Brownscher Bewegung (The theory of drop and rise tests on Brownian motion particles), Phys. Z. **16**, 289 (1915).
[39] T. Schwalger, K. Fisch, J. Benda, and B. Lindner, How noisy adaptation of neurons shapes interspike interval histograms and correlations, PLoS Comput. Biol. **6**, e1001026 (2010).
[40] T. Schwalger and B. Lindner, Theory for serial correlations of interevent intervals, Eur. Phys. J. Spec. Top. **187**, 211 (2010).
[41] F. Gabbiani and C. Koch, Principles of spike train analysis, in *Methods in Neuronal Modeling: From Synapses to Networks*, edited by C. Koch and I. Segev (MIT Press, Cambridge, MA, 1998), Chap. 9, pp. 313–360.
[42] M. J. E. Richardson, Spike-train spectra and network response functions for non-linear integrate-and-fire neurons, Biol. Cybern. **99**, 381 (2008).
[43] W. Bair, C. Koch, W. Newsome, and K. Britten, Power spectrum analysis of bursting cells in area MT in the behaving monkey, J. Neurosci. **14**, 2870 (1994).
[44] R. D. Vilela and B. Lindner, Comparative study of different integrate-and-fire neurons: Spontaneous activity, dynamical response, and stimulus-induced correlation, Phys. Rev. E **80**, 031909 (2009).
[45] D. R. Cox and P. A. W. Lewis, *The Statistical Analysis of Series of Events* (Chapman and Hall, London, 1966).
[46] T. Schwalger, D. Miklody, and B. Lindner, When the leak is weak - how the first-passage statistics of a biased random walk can approximate the ISI statistics of an adapting neuron, Eur. Phys. J. Spec. Top. **222**, 2655 (2013).